JACS
JOURNAL OF THE AMERICAN CHEMICAL SOCIETY

Article

pubs.acs.org/JACS

Macromolecular Crystallography for Synthetic Abiological Molecules: Combining xMDFF and PHENIX for Structure Determination of Cyanostar Macrocycles

Abhishek Singharoy,[†,⊥] Balasubramanian Venkatakrishnan,[‡,⊥] Yun Liu,[§,⊥] Christopher G. Mayne,[†] Semin Lee,[§,#] Chun-Hsing Chen,[§] Adam Zlotnick,*[,‡] Klaus Schulten,*[,†,∥] and Amar H. Flood*[,§]

[†]Beckman Institute for Advanced Science and Technology, University of Illinois at Urbana−Champaign, 405 North Mathews Avenue, Urbana, Illinois 61801, United States

[‡]Molecular and Cellular Biochemistry Department, Indiana University, 212 South Hawthorne Drive, Bloomington, Indiana 47405, United States

[§]Department of Chemistry, Indiana University, 800 East Kirkwood Avenue, Bloomington, Indiana 47405, United States

[∥]Department of Physics, University of Illinois at Urbana−Champaign, 1110 West Green Street, Urbana, Illinois 61801, United States

Supporting Information

ABSTRACT: Crystal structure determination has long provided insight into structure and bonding of small molecules. When those same small molecules are designed to come together in multimolecular assemblies, such as in coordination cages, supramolecular architectures and organic-based frameworks, their crystallographic characteristics closely resemble biological macromolecules. This resemblance suggests that biomacromolecular refinement approaches be used for structure determination of abiological molecular complexes that arise in an aggregate state. Following this suggestion we investigated the crystal structure of a pentagonal macrocycle, cyanostar, by means of biological structure analysis methods and compared results to traditional small molecule methods. Cyanostar presents difficulties seen in supramolecular crystallography including whole molecule disorder and highly flexible solvent molecules sitting in macrocyclic and intermolecule void spaces. We used the force-field assisted refinement method, molecular dynamics flexible fitting algorithm for X-ray crystallography (xMDFF), along with tools from the macromolecular structure determination suite PHENIX. We found that a standard implementation of PHENIX, namely one without xMDFF, either fails to produce a solution by molecular replacement alone or produces an inaccurate structure when using generic geometry restraints, even at a very high diffraction data resolution of 0.84 Å. The problems disappear when taking advantage of xMDFF, which applies an optimized force field to realign molecular models during phasing by providing accurate restraints. The structure determination for this model system shows excellent agreement with the small-molecule methods. Therefore, the joint xMDFF-PHENIX refinement protocol provides a new strategy that uses macromolecule methods for structure determination of small molecules and their assemblies.

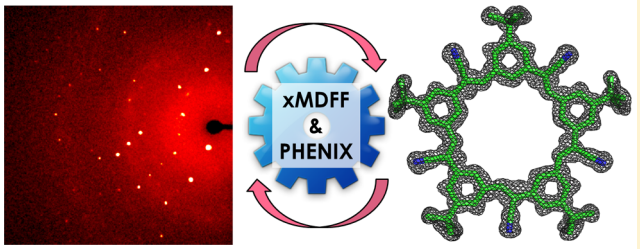

INTRODUCTION

X-ray crystallography[1,2] is an indispensable structure determination tool in the chemical sciences. The structural models that are determined through atomic-scale fitting and interpretation of the extracted electron densities have frequently been used to support or refute the discovery of novel chemical identities,[3] properties,[4] and functions.[5] The protocols[6] that are used to determine the crystal structures of small molecules can transform reciprocal space X-ray diffraction data sets into real space electron density. When confronted with lower resolution, such as can occur when small molecules are brought together in supramolecular architectures, like coordination cages,[7] abiological foldamers,[8] metal-organic frameworks[9] and covalent-organic frameworks,[10−12] traditional small-molecule protocols will be challenged. In such many-molecule assemblies, the crystal packing and diffraction data are more typical of biological macromolecules.

As a consequence of interest in the structure and packing of large multimolecule assemblies, a crossover region between small molecules and biological macromolecules has emerged.[13] For instance, the crystals of coordination cages[7] have a range of characteristics: asymmetric units with dimensions around 10 000 Å^3, whole unit cells that often contain as many as 48 repeating units, and which contain greater regions of disorder, often a natural consequence of solvent filling void spaces in the multimolecule architecture. The stated features render ab initio structure modeling from electron density peaks difficult.

Received: April 28, 2015
Published: June 29, 2015

DOI: 10.1021/jacs.5b04407
J. Am. Chem. Soc. 2015, 137, 8810−8818

Recognition of this crossover region motivated our investigation into the use of macromolecular methods[14] for the structure determination of the abiological molecule, cyanostar[15] (Figure 1). Cyanostar, while being a small molecule (MW ~

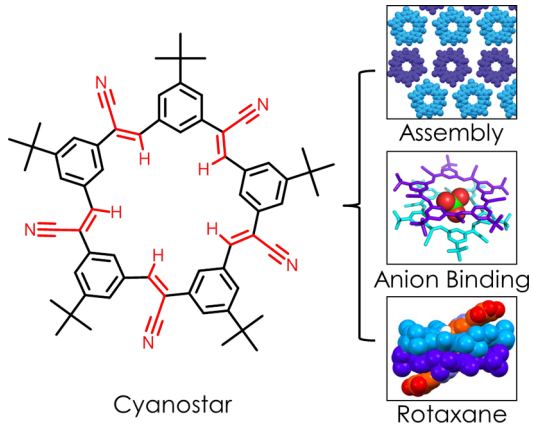

Figure 1. Chemical structure of the cyanostar macrocycle and an overview of its supramolecular chemistry.

900 D), exhibits whole-molecule disorder, dimerizes in the solid state (unit cell ~1800 D) and bears weakly ordered solvents in and around its binding pocket. Comparison to the structure[15] determined with small-molecule methods[6] showed that the crossover region between small and large molecules can benefit greatly from a combination of PHENIX and xMDFF, methods extended herein for use in abiological macromolecular structure determination.

The principles underlying small-molecule and macromolecular crystallography are essentially the same, however, approaches and software implementations distinguish the two fields of crystallography from each other. Small molecule crystallography is usually devoted to small (<2000 D), relatively rigid molecules that diffract to high resolution (<1.0 Å) whereas macromolecular crystallography may extend to mega-Dalton complexes, e.g., ribosomes and viruses, which also have often substantial regions of disorder. Unlike small molecule approaches (Figure 2a), macromolecular strategies (Figure 2b) involve bootstrapping phase information as a means to obtain an initial electron density map[14,16] and then relying on prior knowledge of widely accepted amino acid and nucleotide geometries to refine these phases.[17] Initial phases are most often estimated from the use of a related molecular model that is placed in the unit cell, a method known as molecular replacement,[14] or from a perturbation of the diffraction pattern by making use of heavy atoms or anomalous scatterers.[16] In essence, the data resolution obtained in the case of small molecules allows the phase to be very well solved and refinement proceeds to bring observed and calculated structure factors into agreement. For macromolecular crystallography, even the initially obtained phase will require a significant amount of optimization during the subsequent refinement process.

A crossover region can be operationally defined by the overlap between where the resolution regimes for small molecule and macromolecular structure determination. For instance, the ultrahigh-resolution structures of proteins (0.48 Å)[18] and nucleic acids (0.55 Å)[19] match small molecules while the data resolution of mesoporous materials built from small molecules can be as high as 1.8 Å.[7] The popular SHELX suite

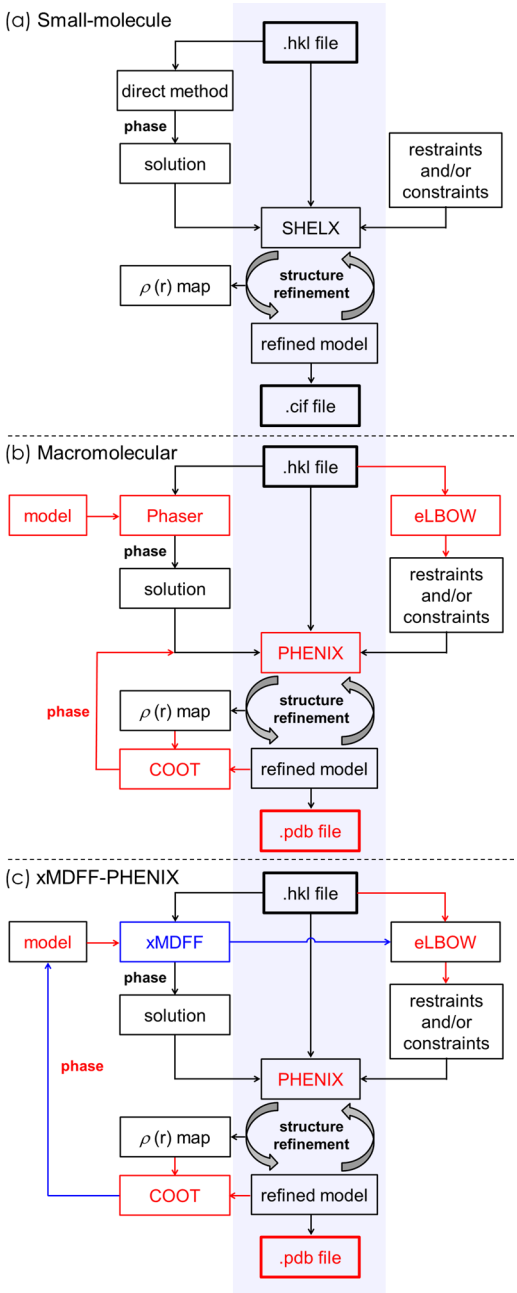

Figure 2. Typical refinement procedures of (a) small-molecule crystallography, (b) macromolecular crystallography and (c) the xMDFF-PHENIX abiological macromolecular crystallography developed here. Differences between small-molecule and macromolecular crystallography are highlighted in red; modifications by xMDFF are in blue.

of programs,[20] originally designed for small molecules, has also been successfully applied to macromolecular crystallography,[21] mainly to identify positions of anomalous scatterers. However, use of the methods for macromolecule structure determination has only rarely been applied to small molecules. Generally, macromolecular methods benefit from the narrow chemical diversity of biological molecules, such as amino and nucleic acids. Thus, the wide availability of biological moieties enables extensive use of subunit geometries to allow generation of accurate restraints and to help direct the refinement. Use of macromolecular methods in the small molecule regimes require

DOI: 10.1021/jacs.5b04407
J. Am. Chem. Soc. 2015, 137, 8810−8818

a means to tackle the extreme chemical diversity present in small molecules.

One seminal effort by Rissanen, Jaskolski and Szumna[13] targeted the structure determination of a 2800-D resorcin[4]-arene dimer using a hybrid approach that began with macromolecule methods and ended with small-molecule techniques. To provide a viable solution to the phase problem, a program used for molecular replacement (PHASER)[22] enabled various molecular models to be inspected. These models included ones from geometry optimized molecular mechanics calculations and from molecular fragments based on the ~1000 crystal structures of resorcin[4]arene. A backbone, tailored from a pre-existing crystal structure of a resorcin[4]-arene analogue,[23] was used as a model to obtain an initial structure solution. This solution was used in a small-molecule-based refinement employing the software SHELXH. Overall, this hybrid strategy relies upon the availability of credible models for molecular replacement and thus may not be readily generalized when applied to novel chemical compounds and their assemblies. Cyanostar is one such example where no crystal structures existed prior to its first disclosure[15] and where every atom in the unit cell is disordered.

Interest in cyanostars (Figure 1) arises from their pentagonal geometry, anion binding pocket,[15] template-directed formation of [3]rotaxanes and anion-responsive 2D crystalline monolayers.[24] Yet, its crystal packing has stretched the limits of small-molecule crystallography. The crystal structure determination of cyanostar offered particular challenges on account of whole molecule disorder.[15] Specifically, the *M* and *P* enantiomers, which arise from cyanostar's bowl chirality,[25] were found to reside in the same unit cell positions with no crystallographic symmetry relating the enantiomers to each other. As a consequence, the electron densities of the *M* and *P* macrocyclic enantiomers overlap each other. The same type of whole molecule disorder was observed in the crystal structures of the [3]rotaxane[15] and for the sandwich complex formed around the ClO_4^- anion.[24]

One approach to overcome the challenges associated with the chemical diversity of abiological molecules involves the assistance of computational models. A recently developed molecular dynamics (MD)-based crystallographic refinement tool xMDFF[26,27] (molecular dynamics flexible fitting[28−30] for X-ray crystallography) offers such a solution and one that is complementary to other small-molecule methods.[31−34] MD and simulated-annealing algorithms have a long history for facilitating structure determination from low-resolution diffraction data sets.[35,36] In addition, xMDFF can be used with PHENIX,[37] a standard package used in macromolecular crystallography. With xMDFF (Figure 2c), real-space refinement is utilized for fitting a molecular model into an iteratively updating electron density map that incorporates the phase from the molecular model, provided by an MD simulation, and the structure factors from the X-ray diffraction data. This algorithm allows force fields to impose chemical correctness during the fitting process. On account of its MD basis, xMDFF provides the necessary sampling of bond lengths, angles and dihedrals, which are required to flexibly fit a molecular model into an electron density map. The power of xMDFF in macromolecular crystallography comes from the ability to accommodate large-scale deformations from the initial structure during the refinement process. These benefits could also play a role in the structure determinations of abiological macromolecules.

To evaluate the usefulness of macromolecular structure determination for synthetic abiological molecules, we used the original data set available from small-molecule crystallography[15] to redetermine the structure of cyanostar. For this purpose we developed a combined xMDFF-PHENIX approach (Figure 2c) to determine the structure. We were able to directly compare the structures obtained from the two methods to assess the accuracy of the macromolecule approach, and its ability to identify and then address whole molecule disorder as well as disordered solvent molecules. The results accurately match those obtained with traditional direct methods for determining the structure of cyanostar and for describing its disorder. By taking advantage of eLBOW (electronic ligand builder and optimization workbench), a module[38] from the PHENIX suite that uses a force-field potential to calculate geometrical restraints for enzyme-bound substrates and ligands, a seamless gateway exists for merging xMDFF with PHENIX-based refinement of abiological macromolecules.

METHODS

The crystal structure of cyanostar macrocycle used for the development of xMDFF-PHENIX has been published previously (CCDC deposition No. 921153). All charges and bond, angle, and dihedral parameters missing from the CHARMM General Force Field (CGenFF)[39] were optimized on model compounds, which are structural components of the cyanostar macrocycle, using the Force Field Toolkit plugin (ffTK)[40] in VMD. An xMDFF-PHENIX-based refinement protocol was employed to resolve the cyanostar crystal structure. All MD simulations were performed in vacuum utilizing CGenFF with parameters developed here for cyanostar employing the ffTK plugin. More details regarding the parametrization and refinement methods are included in the Supporting Information. Programs are available online: PHENIX at http://www.phenix-online.org; xMDFF at http://www.ks.uiuc.edu/Research/mdff/documentation.html; and the ffTK plugin (version 1.1) at http://www.ks.uiuc.edu/Research/vmd/plugins/fftk/.

RESULTS AND DISCUSSION

Crystallographic Refinement of Cyanostar. The structure determination of cyanostar was investigated using various standard and new approaches. Initially, the default routines (Figure 2b) in PHENIX were used. However, application of molecular replacement (PHASER) to the cyanostar structure determination by using the approach followed by Rissanen, Jaskolski and Szumna[13] did not even yield a solution. Presumably the high degree of local disorder in the crystal caused PHASER to experience difficulties when attempting to match the cyanostar model to the diffraction data, even when the model was on the correct site. To circumvent PHASER, the cyanostar model was directly placed in the location where the local electron density map matched best the shape of a macrocycle. Nevertheless, when following this modified approach and using restraints generated within eLBOW (Figure 2b), the refinement of the cyanostar structure (Figure 3a) failed to generate the expected planarity. Refinement artifacts seemed to distort the electron density map and the resulting molecular structure. Consistent with these assessments of the poor match to the correct structure, the *R*-factor R_{work} was on the order of 0.6, indicating that the model cannot be necessarily distinguished from a random distribution of atoms. The interpretation of R_{work} resembles the R_1 parameter from small-molecule crystallography.[41] This high value for R_{work} is acknowledged by macromolecular crystallog-

DOI: 10.1021/jacs.5b04407
J. Am. Chem. Soc. 2015, 137, 8810−8818

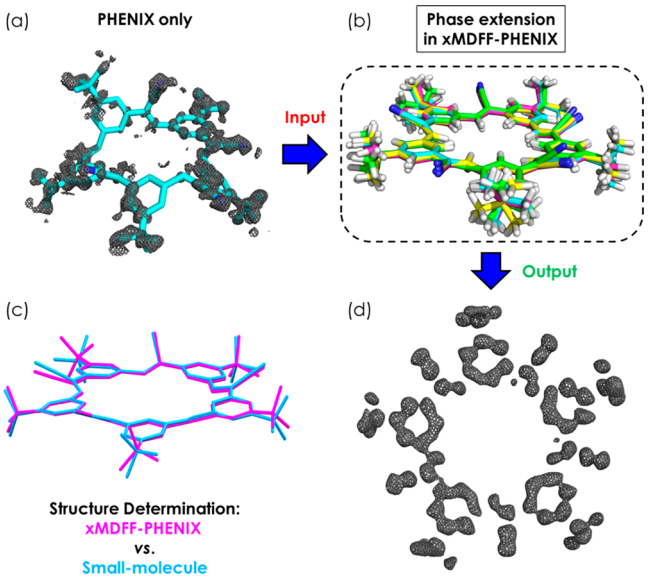

Figure 3. (a) Distorted cyanostar structure from refinement using PHENIX alone. This structure was used subsequently as the input model for xMDFF-PHENIX refinement. (b) Structures are shown at different stages of phase extension based on data at various resolution cut-offs: 3 Å in yellow, 2 Å in magenta, 1.5 Å in cyan and 0.84 Å in green. (c) The structure of cyanostar (magenta) determined by xMDFF-PHENIX shows good agreement with the structure (cyan) refined by the small molecule method. (d) The improved electron density map (gray mesh, 1.5σ contour) clearly matches well with a single cyanostar macrocycle.

raphers to signify a cutoff value beyond which it is not possible to obtain a structure solution.

A successful determination was only possible when using xMDFF. First, structural restraints were computed from force field parameters that are generated by ffTK and implemented in xMDFF. Second, the combination of these structural restraints with the structural solution obtained from the standard PHENIX protocol (Figure 3a) ultimately led to successful phase determination with ordered electron density (Figure 3d). In this case, both *R*-factors (R_{work} and R_{free})[41] were within normal limits for standard structure determinations.

It is critical to ensure that any refinement process is not trapped in a local minimum but rather achieves a globally optimized structure that is consistent with the diffraction data. Phase extension is a standard approach used in macromolecular crystallography to help funnel the optimization while minimizing model bias, especially when the starting model is not ideal. To implement this approach, molecular replacement by the model was repeated by starting the phase determination at low resolution: the diffraction data was artificially truncated to 3 Å and then followed by stepwise phase extension to 0.84 Å. We found that phase extension helped particularly to resolve the positions of the outward directed cyano groups and the three methyl groups that constitute the *t*-butyl substituents, both of which showed the most changes during phase extension (Figure 3b). Refinements conducted at various data resolutions revealed an atomically well-resolved cyanostar core constituted by the inner 25-membered ring. Interestingly, during the phase extension in the range of 3.0 to 0.84 Å resolution, root-mean-square deviations (RMSDs) of the 25-membered ring relative to that of the cyanostar's structure refined with small molecule techniques[15] increased from 0.13 to 0.26 Å, respectively. In contrast, the entire cyanostar macrocycle exhibited RMSDs that decreased (0.48−0.34 Å) across the same range even though they are higher in magnitude. Although the peripheral *t*-butyl substituents on the phenyl rings lead to higher overall RMSD values compared to those of the rigid core, the decrease of the overall RMSDs must be attributed to improved modeling of the rotatable *t*-butyl substituents.

The overall cyanostar macrocycle obtained by xMDFF-PHENIX (Figure 3c, magenta) shows high consistency with the structure refined by small-molecule approaches (Figure 3c, cyan). The low RMSDs are a testament to the ability of xMDFF, enabled by a robust force field, to model flexibly and thus to be capable of refining systematically the cyanostar structure during phase extension. In comparison, the problematic PHENIX-only refined model (Figure 3a) showed a large RMSD of 2.1 Å relative to the structure refined with xMDFF-PHENIX (Figure 3c). This significant difference is another testament to the large-scale deformations xMDFF utilizes to reconcile trial models with diffraction data.

Starting with the PHENIX-only refined model that showed an R_{work} >60%, initial rounds of xMDFF-only refinement with data truncated to a 3-Å resolution reduced R_{work} to ∼45%. Removal of hydrogen atoms further improved R_{work} to ∼35%. When xMDFF refinements were followed by iterative real-space position and *B*-factor refinement in PHENIX, additional improvements lead to an R_{work} value of 34%. When occupancies were assigned to *M* and *P* isomers (63:37) in the electron density based on occupancies from previous studies,[15] further refinement with PHENIX generated an R_{work} value of 29%. (An independent assessment of the *M*/*P* occupancies was also undertaken, vide infra.) Hydrogen atoms were added back at this stage, which improved R_{work} to 27%. The final round of refinement accounted for interatomic scattering.[42]

The existence of whole-molecule disorder with cyanostar introduced complications at various stages of the refinement process, including the refinement of atomic positions at the initial stage where the *R*-factor plateaued at about 45%. We speculated that hydrogens were restricting the refinement algorithm by increasing the volume of the model and removal of hydrogen atoms would allow the program to focus on the heavier atoms first. Indeed we found this approach helped the refinement and lowered the *R*-factor. Once proper atomic positions were established and the whole-molecule disorder was resolved by occupancy refinement, adding back the hydrogen atoms improved the *R*-factor, as expected.

The remainder of the unit cell's composition was then determined. In accordance with the $P\bar{1}$ symmetry of the unit cell, the second macrocycle that is related by an inversion center to the first one was clearly observed in the electron density map by the end of the xMDFF-only refinement stage. The second cyanostar was then included to complete the construction of the model. Subsequent cycles of xMDFF-PHENIX refinement that start from this model revealed diffusive electron density that can be accounted for by two molecules of diglyme, a solvent that was used in the crystallization of cyanostar (Figure 4b,c). The first diglyme was bound inside two stacked cyanostar macrocycles and thus formed a 2:1 complex in the solid state. Another diglyme, which was *not* identified by the small molecule refinement, was found and seen to sit roughly parallel to these 2:1 complexes, running from the bottom of one complex to the top of another (Figure 4a). Both diglyme molecules are located in special positions, i.e., having their molecular centers coinciding with

DOI: 10.1021/jacs.5b04407
J. Am. Chem. Soc. 2015, 137, 8810−8818

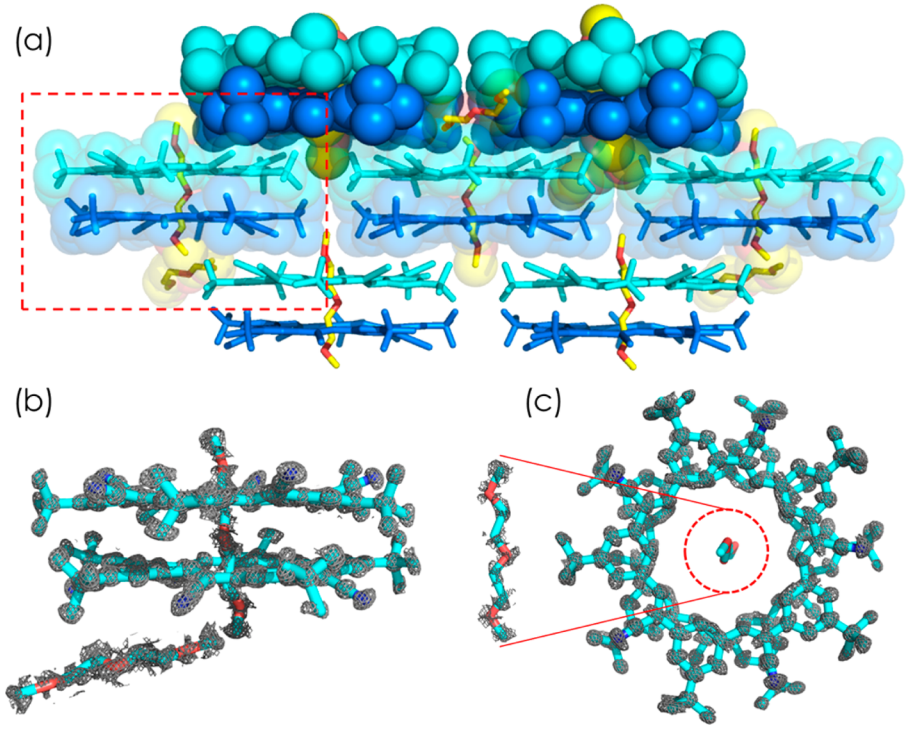

Figure 4. (a) Lamellar packing of cyanostar-diglyme sandwiches in the crystal. The cyanostar dimers are colored in blue and cyan, the diglymes in yellow with their oxygen atoms in red. Hydrogen atoms are omitted for clarity. The red box highlights the chemical components of one unit cell constituted by (b, c) a cyanostar dimer (1.5σ electron density contour) and two diglyme solvent molecules (0.5σ electron density contour).

the inversion centers. On account of the fact that there are two diglymes in one unit cell, they occupy two of the eight independent inversion centers: the cell origin, three face centers, three axis centers and the body center (Figure S7). The bound diglymes are located on the centers of four symmetry-related cell axes (*a* in this case), while unbound diglymes are located on two symmetry-related face centers (*ac* plane in this case). Overall, both the 2:1 complexes and the unbound diglymes are aligned approximately parallel to the face diagonal direction of the *bc* planes of the unit cell with the macrocycles' π surfaces tilted along the diagonal axis. Although both diglymes could potentially have occupancy values smaller than one, they are not refined on account of their high degree of disorder. Alternatively, one could attribute the diffusiveness of the diglyme electron density to disorder and partial occupancy; these two factors cannot be distinguished here.

The final *R*-factors achieved (R_{work} = 25% and R_{free} = 28%) were surprisingly high for the final data resolution used in the structure refinement (0.84 Å). *R*-factors are dependent on data resolution and were seen to increase, i.e., get worse, with improving resolution. The scale factor,[41] which relates the observed structure factors to the calculated structure factors, deviated from an expected value of 1.0 in the high data resolution range (1−0.84 Å). Thus, disorder can contribute to the high *R*-factors. Conversely, the Pearson correlation coefficients CC_{work} and CC_{free}, which provide a measure of the linear correlation between F_{calc}^2 and F_{obs}^2 (peak intensities), were found to have reasonable values of 98.4 and 94.2%, respectively. These high percentages suggest that the diffraction data was nicely fitted by our model, which is in an good agreement with the low RMSD of 0.3 Å between the small molecule and macromolecular methods, thereby enhancing our confidence in the atomic accuracy of the analysis.

The fact that R_{work} is high may be rationalized by comparing our molecular system to most protein structures. In addition to the disordered solvent molecules, the macrocycle exhibits whole molecule disorder in the crystal; every single one of the atomic scatterers is disordered. The presence of whole molecule disorder in a crystal can lead to worsened *R*-factors in the 1−0.84 Å resolution regime where the information on interatomic periodicity is stored. Although protein crystals can also have a large quantity of disordered solvent molecules, the protein backbone is not usually subject to whole molecule disorder. As a result, the resolution-dependent R_{work} is more adversely affected in the 1−0.84 Å resolution range for the cyanostar sample when compared to many protein structures. Correlation coefficients directly compare the model with the data and are not resolution-dependent. Thus, CC_{work} and CC_{free} better describe the quality of the xMDFF-PHENIX refinement of the cyanostar structure.

Whole Molecule Disorder. The difference map ($F_{obs}-F_{calc}$) for the crystal structure of cyanostar obtained after xMDFF-PHENIX refinement shows positive densities (Figure 5a, black mesh) corresponding to a stereoisomer of cyanostar not defined by crystallographic symmetry. This positive density is indicative of whole molecule disorder. As observed from previous studies,[15] the cyanostar macrocycle is not perfectly flat and is better described as a shallow bowl. When viewed down the C_5 symmetry axis and when looking down into the "bottom" of the bowl,[25] two directions can be identified. Using priority rules by starting at the phenyl ring, stereochemical assignment is based on the location of the nearest cyano group: the *P* isomer runs clockwise and *M* isomer counterclockwise (Figure 5b). The averaged electron density from the superposition of *M* and *P* isomers at the same crystallographic location is only restricted by the overall crystallographic symmetry of $P\bar{1}$. Even though the symmetry would suggest

DOI: 10.1021/jacs.5b04407
J. Am. Chem. Soc. 2015, 137, 8810−8818

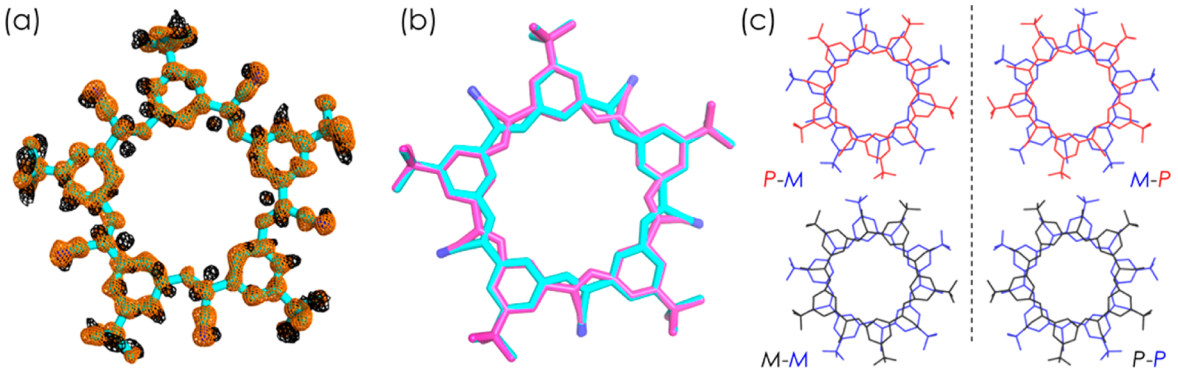

Figure 5. Whole molecule disorder of cyanostar macrocycles. (a) The unaccounted electron density (black mesh) shown in the difference map (F_0–F_c, 1.5σ contour) clearly constitutes a second complete cyanostar macrocycle that is crystallographically different from the already modeled electron density (orange mesh) presented in the data-weighted difference map of $2F_0$–F_c (1.5σ contour). (b) Two cyanostar stereoisomers coexist at the same crystallographic location: the major electron density (orange mesh) translates to an *M* isomer (cyan tube model), and the minor electron density (black mesh) to a *P* isomer (magenta tube model). (c) Four possible stereoisomers of a cyanostar dimer that can be present in the crystal (the first letter indicates the top layer).

that the distribution of *M* and *P* isomers at the location of the first macrocycle within the stacked dimer should be a mirror image of the second macrocycle, symmetry is defined by the *average* of every single unit cell in the crystal. Thus, the whole molecule disorder exists on both sites and it precludes differentiation between cases where the dimer is composed of either randomly paired enantiomers (*P*–*P*, *M*–*M* and *M*–*P*) or the two enantiomers that are actually stacked as an *M*–*P* racemic sandwich (Figure 5c).

To refine whole molecule disorder, another set of *M* and *P* isomers were added to the electron density map right on top of the existing *P*–*M* dimer model, where each of these extra macrocycles shares the same location with its stereoisomer. For instance, a *P* isomer will be added to locations where an *M* isomer exists. All the atoms in one macrocycle are grouped to share a single occupancy value. The occupancy ratio between isomers was refined to be 69:31 for *M*:*P* at one position and *P*:*M* at the other position related by an inversion center. This ratio is in agreement with the distribution of cyanostar enantiomers previously determined (63% *M* and 37% *P*) from the small-molecule studies.[15] The 69:31 ratio was used in the final refinement that achieved the R_{work} of 25%.

The differences in refinement strategies between macromolecular and small molecule methods likely produced the small differences in observed in *M*:*P* distribution values. In the small molecule refinement, atoms from two disordered portions that are too close to each other would sometimes be assigned by the crystallographer to have the same coordinates. If this approach is not taken, anisotropy refinement of these two atoms could result in negative electron densities. While this strategy helps prevent negative densities during anisotropy refinement, it will also occasionally yield structural distortions.[15] In contrast, human bias is reduced to a very limited degree in our xMDFF refinement on account of the fact that the MD simulations refined the "two" cyanostars on the same location independently. This equal treatment allows the minor copy of the macrocycle to be freed from overlaps with the major one and refined independently using the same sets of restraints. This independence assured that the two enantiomers are chemically identical, an idea we can evaluate from the structural data. As a consequence, one would anticipate the two enantiomers would have very similar structural parameters after full refinement, such as bond angles (Figure 6a).

We assessed the expectation that the xMDFF approach will yield greater similarity between the *M* and *P* stereoisomers sitting on the same crystallographic site. We compared internal C–C–C bond angles around the rigid benzene rings, structural features that may reasonably be expected to be the same. First, each of the six internal angles of the benzene moieties was compared across all five rings resulting in six intramolecular comparisons for the major (Figure 6b) and six for the minor (Figure 6c) enantiomer. Although the angles within a single benzene will deviate from the ideal 120° on account of substitution, one would expect that this deviation pattern would be repeated on each of cyanostar's five benzene rings. Second, we compared the same sets of chemically equivalent internal angles but this time between the *M* and *P* enantiomers that occupy the sites of whole molecule disorder resulting in 30 intermolecular comparisons (Figure 6d). In this case, two benzene rings from the two colocated enantiomers would be expected to share the same deviation pattern particularly for those that are close in space. The same analyses were conducted on the structure resolved by small-molecule method (Figure 6e–g).

In this similarity assessment, the small molecule approach shows deviations of up to ±7° for both the intramolecular and intermolecular comparisons (Figure 6). These deviations are five times larger than when using xMDFF-PHENIX (±1.4°) (Figure 6). These observations indicate that the use of xMDFF, which allows each molecule to be treated independently, appears to increase structural similarity between chemically equivalent moieties when addressing whole molecule disorder. When considering the macromolecule refinement alone, the intermolecular deviation (Figure 6b,c) was found to be two times greater than the intramolecular deviation (Figure 6d). This finding suggests that xMDFF-PHENIX approach is ultimately limited by the fact that the major macrocycle has twice the amount of data than the minor one, leading to structural differences between colocated enantiomers.

xMDFF-PHENIX Method for Abiological Macromolecular Crystallography. The PHENIX suite had been originally designed for automated structure determination for biological macromolecules.[43] PHENIX already includes features designed for incorporating nonbiological molecules into macromolecular structures, which allow it to be used in abiological macromolecule structure determination. These features include the

DOI: 10.1021/jacs.5b04407
J. Am. Chem. Soc. 2015, 137, 8810–8818

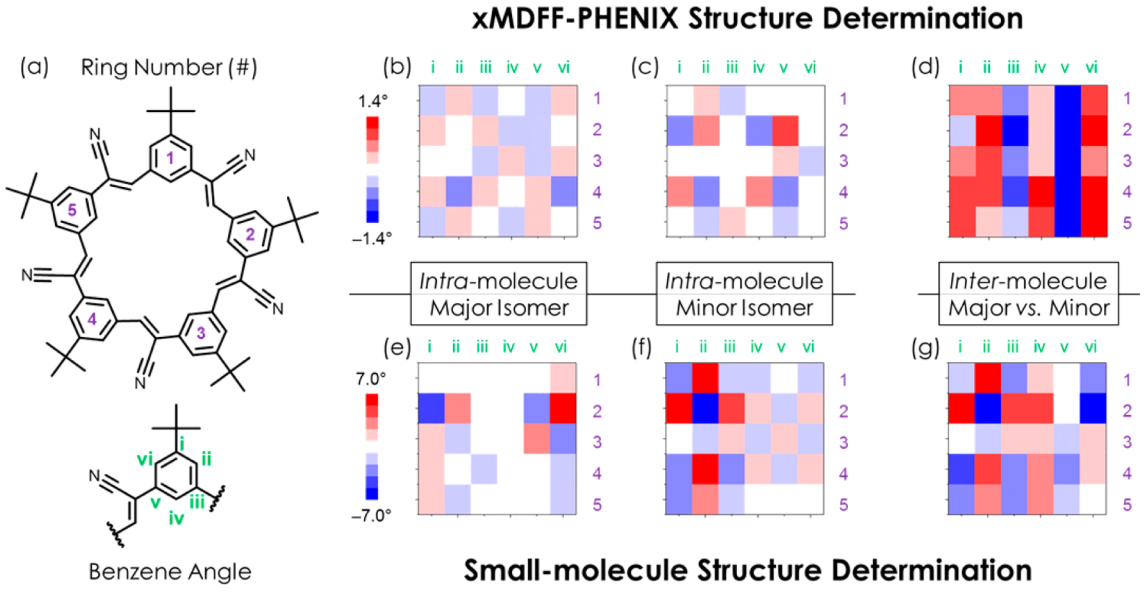

Figure 6. (a) Cyanostar macrocycle with its five repeating aromatic rings (1 to 5) and each phenyl ring with six internal C−C−C bond angles (i to vi). Cyanostar macrocycle resolved by the xMDFF-PHENIX approach shows (b−d) smaller structural distortions (±1.4°) than when resolved by (e−g) the small molecule approach (±7°). The analysis is performed by comparing how the C−C−C bond angles vary between benzene rings within the same macrocycle and between enantiomers that are present at the same location. The deviations are measured by angles (degree). For the 2D plots of major or minor isomers, a column represents how a particular angle (i to vi) varies from one phenyl to another across one macrocycle (1 to 5). The average of one particular angle over five phenyl rings is used as the zero-point reference to define positive (red) and negative (blue) deviations. The 2D plots for major vs minor are created by subtracting angles of the minor copy from the same ones located in the phenyl rings of the major copy that are closest in space.

following two components: (i) the eLBOW module uses force fields to energy minimize chemical structures and to generate restraints for the refinement process; (ii) REEL (restraints editor especially ligands) can be used as a restraint viewer, which permits convenient modification of bond, angle and dihedral values for structures with noncanonical stereochemistry (i.e., deviating from the standard biological moiety library). When eLBOW and REEL are used in conjunction with accurate and robust force fields computed by ffTK and applied through xMDFF's refinement protocols, abiological macromolecular crystallography can be achieved as we have shown here. This outcome holds true despite the large extent of disorder present in every single atom in the crystal. For the crystalline form of cyanostar, its whole molecule disorder can be clearly observed in the electron density map (Figure 5a), which allowed a basis to identify and include it in the refinement. The successful use of xMDFF-PHENIX with cyanostar demonstrates the ability of this method to address structure determination challenges in the crossover area occupied by large and multimolecule assemblies.

Application of an accurate force field is important for ensuring that each xMDFF performance is consistent, e.g., during the many cycles of refinement of the abiological system considered here. In addition, MD simulations are known to be critical for increasing the radius of convergence of real-space refinements.[35] In our case, the initial model differs from the final cyanostar structure by a large RMSD of 2.1 Å (Figure 3a). Thus, use of MD simulations was necessary to drive the poor initial model toward a structure solution that is more consistent with the diffraction data. Such application of MD simulations will become more important when the crystallized compound is unknown, in which case extended sampling (longer MD simulations) will be required. Once the refinement has reached the final stages, MD simulations can be replaced with energy minimizations.

On account of our generalized workflow (Figures 2c and S6) and on the strength of the results achieved for cyanostar, we suggest that crystal structure determination at various size scales can be done with the xMDFF-PHENIX protocol. For traditional macromolecular crystallography, carefully parametrized force fields would be useful for dealing with odd geometries from exotic prosthetic groups, ligands or binding partners, and is well within the purview of the ffTK program. More generally, xMDFF-PHENIX can be applied to multimolecular and abiological macromolecules. We believe that this protocol will also be useful for identifying functional polymorphs, such as in cases where a polymorphic crystal may diffract with low resolution, which would normally preclude further structural interpretation.

■ CONCLUSIONS

The present study emphasizes the critical element of utilizing an accurate force field for restraint-based crystal structure determination and shows how such a force field can form the basis for abiological macromolecular crystallography. The software suites used for traditional macromolecular structure determination work well for biorelevant macromolecules and architectures with huge molecular weights. However, imperfect force field descriptions for novel abiological structures, even in the case of structures of moderate size, can be a roadblock to general application to abiological macromolecules. The accurate quantum chemical information incorporated into the force field by ffTK is ultimately reflected in the accuracy of the structural features of the system investigated, in the present case, the cyanostar structure solution. These features include the correct geometries achieved for cyanostar and its dimeric form in the unit cell, the modeling of the whole molecule disorder and

DOI: 10.1021/jacs.5b04407
J. Am. Chem. Soc. 2015, 137, 8810−8818

dealing with the disordered diglyme that partially populates the cyanostar dimer's binding pocket. The workflow developed here makes use of an xMDFF-PHENIX hybrid approach and serves as a general starting point for determining structures from data sets that are traditionally found to resist small-molecule methods. Furthermore, the customized force field can also be utilized in characterizing the compound's dynamics. In the long term, xMDFF-PHENIX provides a complementary approach for structure determinations of abiological macromolecules of increasing size and complexity.

■ ASSOCIATED CONTENT

Supporting Information

Survey of challenging crystal structures, force field parametrizations, detailed refinement protocols of xMDFF-PHENIX, and input/output data files. The Supporting Information is available free of charge on the ACS Publications website at DOI: 10.1021/jacs.5b04407.

■ AUTHOR INFORMATION

Corresponding Authors

*azlotnic@indiana.edu
*kschulte@ks.uiuc.edu
*aflood@indiana.edu

Present Address

[#]Beckman Institute for Advanced Science and Technology, University of Illinois at Urbana−Champaign, 405 North Mathews Avenue, Urbana, Illinois 61801, United States.

Author Contributions

[⊥]A.S., B.V., and Y.L. contributed equally to this work.

Notes

The authors declare no competing financial interest.

■ ACKNOWLEDGMENTS

The authors thank Dr. Maren Pink for helpful discussions. A.S., C.G.M. and K.S. acknowledge support from the National Institutes of Health (NIH; 9P41GM104601, 5R01GM098243-02 and U54GM087519). B.V. and A.Z. acknowledge NIH (R01AI067417) for support. A.H.F. acknowledges support from the NSF (CHE1412401). A.S. acknowledges the Beckman Postdoctoral Fellowship. Y.L. thanks the Raymond Siedle Materials Fellowship.

■ REFERENCES

(1) Laue, M. v. *Phys. Z.* **1913**, *14*, 421−423.

(2) Bragg, W. H.; Bragg, W. L. *Proc. R. Soc. London, Ser. A* **1913**, *88*, 428−438.

(3) Watson, J. D.; Crick, F. H. C. *Nature* **1953**, *171*, 731−738.

(4) Flack, H. D.; Bernardinelli, G. *Chirality* **2008**, *20*, 681−690.

(5) Schotte, F.; Lim, M.; Jackson, T. A.; Smirnov, A. V.; Soman, J.; Olson, J. S.; Phillips, G. N.; Wulff, M.; Anfinrud, P. A. *Science* **2003**, *300*, 1944−1947.

(6) Karlé, J.; Hauptmann, H. *Acta Crystallogr.* **1952**, *10*, 267−270.

(7) Selected papers for coordination cages with challenging crystal structures, e.g., asymmetric unit larger than 4000 Å^3: (a) Argent, S. P.; Adams, H.; Riis-Johannessen, T.; Jeffery, J. C.; Harding, L. P.; Ward, M. D. *J. Am. Chem. Soc.* **2006**, *128*, 72−73. (b) Fox, O. D.; Cookson, J.; Wilkinson, E. J.; Drew, M. G.; MacLean, E. J.; Teat, S. J.; Beer, P. D. *J. Am. Chem. Soc.* **2006**, *128*, 6990−7002. (c) Newkome, G. R.; Wang, P.; Moorefield, C. N.; Cho, T. J.; Mohapatra, P. P.; Li, S.; Hwang, S. H.; Lukoyanova, O.; Echegoyen, L.; Palagallo, J. A.; Iancu, V.; Hla, S. W. *Science* **2006**, *312*, 1782−1785. (d) Suzuki, K.; Kawano, M.; Sato, S.; Fujita, M. *J. Am. Chem. Soc.* **2007**, *129*, 10652−10653. (e) Murase, T.; Sato, S.; Fujita, M. *Angew. Chem., Int. Ed.* **2007**, *46*, 5133−5136. (f) McKinlay, R. M.; Atwood, J. L. *Angew. Chem., Int. Ed.* **2007**, *46*, 2394−2397. (g) Mal, P.; Schultz, D.; Beyeh, K.; Rissanen, K.; Nitschke, J. R. *Angew. Chem., Int. Ed.* **2008**, *47*, 8297−8301. (h) Sun, Q. F.; Iwasa, J.; Ogawa, D.; Ishido, Y.; Sato, S.; Ozeki, T.; Sei, Y.; Yamaguchi, K.; Fujita, M. *Science* **2010**, *328*, 1144−1147. (i) Sun, Q. F.; Murase, T.; Sato, S.; Fujita, M. *Angew. Chem., Int. Ed.* **2011**, *50*, 10318−10321. (j) Clever, G. H.; Kawamura, W.; Tashiro, S.; Shiro, M.; Shionoya, M. *Angew. Chem., Int. Ed.* **2012**, *51*, 2606−2609. (k) Pasquale, S.; Sattin, S.; Escudero-Adan, E. C.; Martinez-Belmonte, M.; de Mendoza, J. *Nat. Commun.* **2012**, *3*, 785. (l) Sun, Q. F.; Sato, S.; Fujita, M. *Nat. Chem.* **2012**, *4*, 330−333. (m) Bruns, C. J.; Fujita, D.; Hoshino, M.; Sato, S.; Stoddart, J. F.; Fujita, M. *J. Am. Chem. Soc.* **2014**, *136*, 12027−12034.

(8) Selected papers for foldamers with challenging crystal structures, e.g., R_1 is higher than 10%: (a) Haldar, D.; Jiang, H.; Leger, J. M.; Huc, I. *Angew. Chem., Int. Ed.* **2006**, *45*, 5483−5486. (b) Kelley, R. F.; Rybtchinski, B.; Stone, M. T.; Moore, J. S.; Wasielewski, M. R. *J. Am. Chem. Soc.* **2007**, *129*, 4114−4115. (c) Liu, S.; Zavalij, P. Y.; Lam, Y. F.; Isaacs, L. *J. Am. Chem. Soc.* **2007**, *129*, 11232−11241. (d) Gan, Q.; Ferrand, Y.; Bao, C.; Kauffmann, B.; Grelard, A.; Jiang, H.; Huc, I. *Science* **2011**, *331*, 1172−1175. (e) Ferrand, Y.; Gan, Q.; Kauffmann, B.; Jiang, H.; Huc, I. *Angew. Chem., Int. Ed.* **2011**, *50*, 7572−7575. (f) Kwon, S.; Shin, H. S.; Gong, J.; Eom, J. H.; Jeon, A.; Yoo, S. H.; Chung, I. S.; Cho, S. J.; Lee, H. S. *J. Am. Chem. Soc.* **2011**, *133*, 17618−17621. (g) Gan, Q.; Ferrand, Y.; Chandramouli, N.; Kauffmann, B.; Aube, C.; Dubreuil, D.; Huc, I. *J. Am. Chem. Soc.* **2012**, *134*, 15656−15659. (h) Kudo, M.; Maurizot, V.; Kauffmann, B.; Tanatani, A.; Huc, I. *J. Am. Chem. Soc.* **2013**, *135*, 9628−9631. (i) Hua, Y.; Liu, Y.; Chen, C. H.; Flood, A. H. *J. Am. Chem. Soc.* **2013**, *135*, 14401−14412. (j) Lautrette, G.; Kauffmann, B.; Ferrand, Y.; Aube, C.; Chandramouli, N.; Dubreuil, D.; Huc, I. *Angew. Chem., Int. Ed.* **2013**, *52*, 11517−11520. (k) Pavone, V.; Zhang, S. Q.; Merlino, A.; Lombardi, A.; Wu, Y.; DeGrado, W. F. *Nat. Commun.* **2014**, *5*, 3581. (l) Buratto, J.; Colombo, C.; Stupfel, M.; Dawson, S. J.; Dolain, C.; Langlois d'Estaintot, B.; Fischer, L.; Granier, T.; Laguerre, M.; Gallois, B.; Huc, I. *Angew. Chem., Int. Ed.* **2014**, *53*, 883−887. (m) Chandramouli, N.; Ferrand, Y.; Lautrette, G.; Kauffmann, B.; Mackereth, C. D.; Laguerre, M.; Dubreuil, D.; Huc, I. *Nat. Chem.* **2015**, *7*, 334−341.

(9) Selected papers for MOFs with challenging crystal structures, e.g., asymmetric unit larger than 4000 Å^3: (a) Park, Y. K.; Choi, S. B.; Kim, H.; Kim, K.; Won, B. H.; Choi, K.; Choi, J. S.; Ahn, W. S.; Won, N.; Kim, S.; Jung, D. H.; Choi, S. H.; Kim, G. H.; Cha, S. S.; Jhon, Y. H.; Yang, J. K.; Kim, J. *Angew. Chem., Int. Ed.* **2007**, *46*, 8230−8233. (b) Sumida, K.; Hill, M. R.; Horike, S.; Dailly, A.; Long, J. R. *J. Am. Chem. Soc.* **2009**, *131*, 15120−15121. (c) Inokuma, Y.; Ning, G. H.; Fujita, M. *Angew. Chem., Int. Ed.* **2012**, *51*, 2379−2381. (d) Feyand, M.; Mugnaioli, E.; Vermoortele, F.; Bueken, B.; Dieterich, J. M.; Reimer, T.; Kolb, U.; de Vos, D.; Stock, N. *Angew. Chem., Int. Ed.* **2012**, *51*, 10373−10376. (e) Inokuma, Y.; Yoshioka, S.; Ariyoshi, J.; Arai, T.; Hitora, Y.; Takada, K.; Matsunaga, S.; Rissanen, K.; Fujita, M. *Nature* **2013**, *495*, 461−466. (f) Ikemoto, K.; Inokuma, Y.; Rissanen, K.; Fujita, M. *J. Am. Chem. Soc.* **2014**, *136*, 6892−6895. (g) Kubota, R.; Tashiro, S.; Shiro, M.; Shionoya, M. *Nat. Chem.* **2014**, *6*, 913−918. (h) Tashiro, S.; Umeki, T.; Kubota, R.; Shionoya, M. *Angew. Chem., Int. Ed.* **2014**, *53*, 8310−8315.

(10) COFs are more recent categories of compound having challeging solid state structure determinations: (a) Cote, A. P.; Benin, A. I.; Ockwig, N. W.; O'Keeffe, M.; Matzger, A. J.; Yaghi, O. M. *Science* **2005**, *310*, 1166−1170. (b) Pestov, D.; Murawski, R. K.; Ariunbold, G. O.; Wang, X.; Zhi, M.; Sokolov, A. V.; Sautenkov, V. A.; Rostovtsev, Y. V.; Dogariu, A.; Huang, Y.; Scully, M. O. *Science* **2007**, *316*, 265−268.

(11) Selected papers for COFs where single crystals are available: (a) Uribe-Romo, F. J.; Hunt, J. R.; Furukawa, H.; Klock, C.; O'Keeffe, M.; Yaghi, O. M. *J. Am. Chem. Soc.* **2009**, *131*, 4570−4571. (b) Zhang, Y. B.; Su, J.; Furukawa, H.; Yun, Y.; Gandara, F.; Duong, A.; Zou, X.; Yaghi, O. M. *J. Am. Chem. Soc.* **2013**, *135*, 16336−16339.

(12) Selected papers for COFs where alternative techniques are used to assist the characterization of the structures: (a) Colson, J. W.; Woll,

DOI: 10.1021/jacs.5b04407
J. Am. Chem. Soc. 2015, 137, 8810−8818

A. R.; Mukherjee, A.; Levendorf, M. P.; Spitler, E. L.; Shields, V. B.; Spencer, M. G.; Park, J.; Dichtel, W. R. *Science* **2011**, *332*, 228−231. (b) Bunck, D. N.; Dichtel, W. R. *J. Am. Chem. Soc.* **2013**, *135*, 14952−14955. (c) Dogru, M.; Handloser, M.; Auras, F.; Kunz, T.; Medina, D.; Hartschuh, A.; Knochel, P.; Bein, T. *Angew. Chem., Int. Ed.* **2013**, *52*, 2920−2924. (d) Liu, X. H.; Guan, C. Z.; Ding, S. Y.; Wang, W.; Yan, H. J.; Wang, D.; Wan, L. J. *J. Am. Chem. Soc.* **2013**, *135*, 10470−10474. (e) Oh, H.; Kalidindi, S. B.; Um, Y.; Bureekaew, S.; Schmid, R.; Fischer, R. A.; Hirscher, M. *Angew. Chem., Int. Ed.* **2013**, *52*, 13219−13222.

(13) Wierzbicki, M.; Gilski, M.; Rissanen, K.; Jaskólski, M.; Szumna, A. *CrystEngComm* **2014**, *16*, 3773−3780.

(14) Rossmann, M. G.; Blow, D. M. *Acta Crystallogr.* **1962**, *15*, 24−31.

(15) Lee, S.; Chen, C.-H.; Flood, A. H. *Nat. Chem.* **2013**, *5*, 704−710.

(16) Perutz, M. F. *Acta Crystallogr.* **1956**, *9*, 867−873.

(17) Konnert, J. H.; Hendrickson, W. A. *Acta Crystallogr.* **1980**, *A36*, 344−350.

(18) Schmidt, A.; Teeter, M.; Weckert, E.; Lamzin, V. S. *Acta Crystallogr.* **2011**, *F67*, 424−428.

(19) Brzezinski, K.; Brzuszkiewicz, A.; Dauter, M.; Kubicki, M.; Jaskolski, M.; Dauter, Z. *Nucleic Acids Res.* **2011**, *39*, 6238−6248.

(20) Sheldrick, G. M. *Acta Crystallogr.* **2008**, *A64*, 112−122.

(21) Sheldrick, G. M.; Schneider, T. R. *Methods Enzymol.* **1997**, *277*, 319−343.

(22) McCoy, A. J.; Grosse-Kunstleve, R. W.; Adams, P. D.; Winn, M. D.; Storoni, L. C.; Read, R. J. *J. Appl. Crystallogr.* **2007**, *40*, 658−674.

(23) Kuberski, B.; Szumna, A. *Chem. Commun.* **2009**, *45*, 1959−1961.

(24) Hirsch, B. E.; Lee, S.; Qiao, B.; Chen, C.-H.; McDonald, K. P.; Tait, S. L.; Flood, A. H. *Chem. Commun.* **2014**, *50*, 9827−9830.

(25) Szumna, A. *Chem. Soc. Rev.* **2010**, *39*, 4274−4285.

(26) McGreevy, R.; Singharoy, A.; Li, Q.; Zhang, J.; Xu, D.; Perozo, E.; Schulten, K. *Acta Crystallogr., Sect. D: Biol. Crystallogr.* **2014**, *70*, 2344−2355.

(27) Li, Q.; Wanderling, S.; Paduch, M.; Medovoy, D.; Singharoy, A.; McGreevy, R.; Villalba-Galea, C.; Hulse, R. E.; Roux, B.; Schulten, K.; Kossiakoff, A.; Perozo, E. *Nat. Struct. Mol. Biol.* **2014**, *21*, 244−252.

(28) Trabuco, L. G.; Villa, E.; Mitra, K.; Frank, J.; Schulten, K. *Structure (London, U. K.)* **2008**, *16*, 673−683.

(29) Trabuco, L. G.; Schreiner, E.; Gumbart, J.; Hsin, J.; Villa, E.; Schulten, K. *J. Struct. Biol.* **2011**, *173*, 420−427.

(30) Chan, K.-Y.; Gumbart, J.; McGreevy, R.; Watermeyer, J. M.; Sewell, B. T.; Schulten, K. *Structure (London, U. K.)* **2011**, *19*, 1211−1218.

(31) Shiono, M.; Woolfson, M. M. *Acta Crystallogr.* **1992**, *A48*, 451−456.

(32) Oszlányi, G.; Sütő, A. *Acta Crystallogr.* **2004**, *A60*, 134−141.

(33) Oszlányi, G.; Sütő, A. *Acta Crystallogr.* **2005**, *A61*, 147−152.

(34) Sheldrick, G. M. *Acta Crystallogr.* **2015**, *A71*, 3−8.

(35) Brünger, A. T.; Kuriyan, J.; Karplus, M. *Science* **1987**, *235*, 458−460.

(36) Brünger, A. T.; Adams, P. D.; Clore, G. M.; DeLano, W. L.; Gros, P.; Grosse-Kunstleve, R. W.; Jiang, J. S.; Kuszewski, J.; Nilges, M.; Pannu, N. S.; Read, R. J.; Rice, L. M.; Simonson, T.; Warren, G. L. *Acta Crystallogr.* **1998**, *D54*, 905−921.

(37) Adams, P. D.; Afonine, P. V.; Bunkóczi, G.; Chen, V. B.; Davis, I. W.; Echols, N.; Headd, J. J.; Hung, L.-W.; Kapral, G. J.; Grosse-Kunstleve, R. W.; McCoy, A. J.; Moriarty, N. W.; Oeffner, R.; Read, R. J.; Richardson, D. C.; Richardson, J. S.; Terwilliger, T. C.; Zwart, P. H. *Acta Crystallogr.* **2010**, *D66*, 213−221.

(38) Moriarty, N. W.; Grosse-Kunstleve, R. W.; Adams, P. D. *Acta Crystallogr.* **2009**, *D65*, 1074−1080.

(39) Vanommeslaeghe, K.; Hatcher, E.; Acharya, C.; Kundu, S.; Zhong, S.; Shim, J.; Darian, E.; Guvench, O.; Lopes, P.; Vorobyov, I.; MacKerell, A. D. *J. Comput. Chem.* **2010**, *31*, 671−690.

(40) Mayne, C. G.; Saam, J.; Schulten, K.; Tajkhorshid, E.; Gumbart, J. C. *J. Comput. Chem.* **2013**, *34*, 2757−2770.

(41) R_{work} is defined by the equation: $R_{work} = \sum_{hkl}(||F_{obs}| - K|F_{calc}||)/\sum_{hkl}|F_{obs}|$, where K is the scaling factor, $|F_{obs}|$ is the amplitude of the observed structure factor, $|F_{calc}|$ is the amplitude of the calculated structure factor. For small molecule crystallography, a slightly different way of calculating the R-factor is used as a result of the model-free refinement protocol: $R_1 = \sum_{hkl}(||F_{obs}| - |F_{calc}||)/\sum_{hkl}|F_{obs}|$. The R-factor depends on the actual refinement process. Therefore, a direct comparison between R_1 and R_{work} is unrealistic. R_{free} is calculated using the same equation for a test set of reflections that are not included in the refinement process. The R_{free} is compared to the R_{work} to check for over-refinement and model bias.

(42) Afonine, P. V.; Grosse-Kunstleve, R. W.; Adams, P. D.; Lunin, V. Y.; Urzhumtsev, A. *Acta Crystallogr.* **2007**, *D63*, 1194−1197.

(43) Afonine, P. V.; Grosse-Kunstleve, R. W.; Echols, N.; Headd, J. J.; Moriarty, N. W.; Mustyakimov, M.; Terwilliger, T. C.; Urzhumtsev, A.; Zwart, P. H.; Adams, P. D. *Acta Crystallogr.* **2012**, *D68*, 352−367.

DOI: 10.1021/jacs.5b04407
J. Am. Chem. Soc. 2015, 137, 8810−8818